Plasticizing Silk Protein for On-skin Stretchable Electrodes

Geng Chen, Naoji Matsuhisa, Zhiyuan Liu, Dianpeng Qi, Pingqiang Cai, Ying Jiang, Changjin Wan, Yajing Cui, Wan Ru Leow, Zhuangjian Liu, Suxuan Gong, Ke-Qin Zhang, Yuan Cheng, Xiaodong Chen**

Prof. X. Chen, Ms. G. Chen, Dr. N. Matsuhisa, Dr. Z. Liu, Dr. D. Qi, Dr. P. Cai, Ms. Y. Jiang, Dr. C. Wan, Ms. Y. Cui, Dr. W. R. Leow
Innovative Centre for Flexible Devices (iFLEX)
School of Materials Science and Engineering, Nanyang Technological University, 50 Nanyang Avenue, Singapore 639798
Email: chenxd@ntu.edu.sg
Webpage: http://www.ntu.edu.sg/home/chenxd

Dr. Y. Cheng, Dr. Z. Liu
Institute of High Performance Computing, Agency for Science, Technology and Research (A*STAR), 1 Fusionopolis Way, #16-16 Connexis North, Singapore 138632
Email: chengy@ihpc.a-star.edu.sg

Prof. K. Q. Zhang
National Engineering Laboratory for Modern Silk, College of Textile and Clothing Engineering, Soochow University, Suzhou 215123, China

Dr. S. Gong
Procter and Gamble, Singapore Innovation Center, 70 Biopolis Street, 138547, Singapore

Keywords: biomaterials, silk protein, molecular dynamics simulation, on-skin electronics, stretchable electronics

Abstract

Soft and stretchable electronic devices are important in wearable and implantable applications because of the high skin conformability. Due to the natural biocompatibility and biodegradability, silk protein is one of the ideal platforms for wearable electronic devices. However, the realization of skin-conformable electronic devices based on silk has been limited by the mechanical mismatch with skin, and the difficulty to integrate stretchable electronics. Here we demonstrate silk protein as the substrates for soft and stretchable on-skin electronics. The original high Young's modulus (5~12 GPa) and low stretchability (<20%) are tuned into 0.1~2 MPa, and >400%, respectively. This plasticization is realized by the addition of $CaCl_2$ and ambient hydration, whose mechanism is further investigated by molecular dynamics simulations. Moreover, highly stretchable (>100%) electrodes are

obtained by the thin-film metallization and the formation of wrinkled structures after ambient hydration. Finally, our plasticized silk electrodes, with the high electrical performance and skin conformability, achieved on-skin electrophysiological recording comparable to that by commercial gel electrodes. Here proposed skin-conformable electronics based on biomaterials will pave the way towards the harmonized integration of electronics into human.

Stretchable electronics is particularly suitable for the application of wearable and implantable devices for healthcare monitoring.[1-5] Unlike conventional bulky electronic systems, soft and stretchable electronic devices have similar mechanical properties with soft human organs including brain and skin.[6-10] In case of on-skin applications, these devices can realize conformable contacts to the arbitrarily shaped and moving skin,[7,11] whose Young's modulus is 0.1 ~ 2 MPa and stretchability is 30 ~ 70%.[12] Therefore, stretchable on-skin healthcare sensors can realize reduced discomfort of wearing and improved signal fidelity, even during motion.[3,17-19] For example, there have been demonstrations of stretchable on-skin healthcare sensors for pressure,[11,13] temperature,[14] and electrophysiology.[15,16] Furthermore, it is ideal for the devices to acquire biocompatibility for long-term on-skin measurement,[20] and biodegradability for the environmental friendliness.[21,22] Biomaterials are the unique options of materials to provide such functions, which include silk, cellulose, chitin and lignin.[22-26] In particular, silk has been proved to have the versatility into desired formats, such as nanofibers, sponges and thin films with high flexibility, robustness, and optical refractive index.[27-30] These attractive features have been fully utilized in the fields of electronics, optics, and biology.[31-34]

The integration of silk into flexible electronics has realized various devices with desired functions.[33] Flexible silk has been employed in the substrates of transient electronics,[21,35] sacrificial layers of ultra-flexible electronics,[7] dielectrics of transistors[36] and active layers of memristors.[37,38] Moreover, stretchable electronic devices were

developed using a spider silk, which is a fiber-shaped biomaterial with high Young's modulus of 1.4 GPa.[39] Coated with carbon nanotubes, stretchable conducting fibers were realized, whose large resistance change against strain was utilized for strain sensor applications.

However, the range of applications has been limited by the lack of silk materials which possess skin-like softness and the ability to integrate stretchable electronics. There are three issues to be solved. Firstly, the mechanical softness and stretchability of silk protein should be comparable to that of skin. Soft silk-based hydrogels can be considered as possible candidates,[40,41] but they need to be prevented from drying.[42] Thus, the second issue is to control the water content inside silk so that it can remain soft under ambient environment. Thirdly, the process to integrate highly conductive materials with high stretchability on such unconventional substrates needs to be established.[2,43]

Here we demonstrate silk protein as highly stretchable substrates for the on-skin stretchable electrodes (**Figure 1**a, b). This is enabled by controlled plasticization of silk protein to which Ca^{2+} ions were added to render the moisture into silk fibroin film from ambient environment (Figure 1c). The Young's modulus, and stretchability were tuned from 5~12 GPa to 0.149 MPa, and from <20% to >400%, respectively.[24,29] This plasticization was further unraveled by the molecular dynamics simulation. Moreover, highly stretchable (>100%) electrode was realized on this plasticized silk via simply depositing a metal layer. The resistance change (R/R_0) is as small as ~2.45 at 40% strain. Such high performance was obtained by the wrinkles formation during the plasticization process by ambient humidity. Finally, the high feasibility of our electrodes for on-skin bioelectronics was demonstrated in electromyography (EMG) signal recording comparable to commercial gel electrodes. This plasticized silk electrodes can be a platform to integrate with other active elements such as sensors and transistors, achieving multi-functions while obtaining the biocompatibility and biodegradability.

We plasticized the original hard and tough silk fibers into the soft and stretchable films by introducing $CaCl_2$,[44] which is abundant in human body fluid, to silk. Silk fibroin was obtained from *Bombyx mori* silkworm silk. Details are available in methods section in supplementary information. By introducing up to 30 wt% of $CaCl_2$, the Young's modulus dropped from 5~12 GPa[24] to 1.66 MPa under relative humidity of 50% while water content increased to 14.64 wt% (Figure 1d). The stretchability improved from <20%[24] to >400%, which is higher than that of human skin (Figure S1). To further clarify the role of $CaCl_2$ and water in this plasticization process, we controlled the relative humidity while fixing the $CaCl_2$ weight ratio at 15 wt%. As the silk with $CaCl_2$ were incubated at various relative humidity from 43% to 85%, the Young's modulus decreased from 412.67 MPa to 0.149 MPa (Figure 1e). Simultaneously, the water content increased from 6.9 wt% to 30.5 wt% in accordance with the decreased Young's modulus. In this way, mechanical property of silk can be tuned by introducing proper amount of $CaCl_2$ depending on the relative humidity. In our lab in Singapore, the relative humidity is at the range of 60 ~ 70%. Therefore, we performed the following experiments using silk protein with 15 wt% $CaCl_2$, resulting in the Young's modulus of 0.4 ~ 2 MPa, which is comparable to that of human skin.

To better understand the mechanism of this plasticization process in silk, molecular dynamics simulations were performed (**Figure 2**). The mechanical characteristics of silk are predominantly determined by highly crystalline domain (crystallites), and amorphous domain as described in Figure 1c.[45-51] Therefore, we performed simulations on the representative crystallites (Figure 2a-c), and amorphous domain (Figure 2d-f). Methods for constructing the models and simulation can be found in methods section in supplementary information.

The mechanical strength of silk fibroin is mainly dictated by the crystalline domain,[46-50] and weakened by water. This was revealed through analysis of hydrogen bonds and interchain energy on the outmost layer of the crystallite based on intensive molecular dynamics simulations. Crystallites in silk consist of closely packed hexapeptides of Glycine

(G), Alanine (A), Tyrosine (Y), and Serine (S). Typical patterns of hexapeptides inside silk include GAGAGS, GAGAGA and GAGYGA.[46,47] Therefore, we built up crystallites models for these three patterns and analyzed their different structural behaviors in vacuum and in water. In this study, only two extreme conditions (in vacuum (fully de-hydrated), and in water (fully hydrated)) were investigated because these two models have shown the reliability in simulation.[45,51,52] The hydrogen bonds in the outmost layer of GAGAGA crystallite at equilibrium in vacuum (Figure 2a) and water (Figure 2b) are shown. The hydrogen bond number in the analysed outmost layer is 6 in water while it is 10 in vacuum. Similar decrease in hydrogen bond was also obtained in the other structures (GAGAGS, GAGYGA) (Figure S2). Furthermore, the interchain energy of three crystallites in water is higher than that in vacuum (Figure 2c). Here the interchain energy refers to the interaction energy between two chains, described by two-side arrows in Figure 2c, and higher interchain energy implies the weaker binding affinity. For example, the interchain energy of one representative GAGAGA crystallite in water is -176.2 kJ/mol, although that in vacuum is -180.6 kJ/mol. This change is comparable to the previous simulation results explaining the effect of water in mechanical properties of silk.[52,53] Crystallite domain serves as the building block of the silk fibroin, thus the small increase in the interchain energy can strongly weaken the mechanical properties of the whole molecules.[45] The statistical data of hydrogen bonds in all crystallites models can be found in the Table S1, which shows decreased hydrogen bond number in water. These simulations on the crystallites show that the addition of water decreases the crystallites strength, which is consistent with the experimental data showing decreased Young's modulus. In addition, the effect of water with Ca^{2+} ions was also investigated, and their influence on crystallite was negligibly small compared to water without Ca^{2+} ions (Table S2). This simulation reveals that water plays a dominant role in the plasticization process of crystallites.

Furthermore, simulations on the amorphous domain explain that water and Ca^{2+} ions introduce the stretchability by influencing its secondary structures.[51,54] Secondary structures are dimensional structures of protein, including β-sheets, random coils, helices, turns, etc.[46] While β-sheets have relatively strong mechanical properties and are not very extensible, the other secondary structures, such as helices and random coils, possess higher extensibility. The simulation is performed to reveal which secondary structures are dominant in vacuum and in water with Ca^{2+} ions. To simulate the dynamics of protein in water, appropriate number of Ca^{2+} ions need to be added to the system to neutralize the charge of the whole system. Figure 2d and 2e show the representative snapshots of the silk protein in vacuum, and in water with Ca^{2+} ions, respectively. In water with Ca^{2+} ions, there is a smaller number of stiff β-sheets and a larger number of extensible secondary structures than in vacuum. This trend was supported by the time evolution of secondary structure in amorphous domain during the simulation (timeline analysis, Figure S3). Figure 2f shows the quantitative secondary structure ratio at equilibrium in vacuum and in water with Ca^{2+} ions. Ratios of β-sheets in vacuum, and in water with Ca^{2+} ions were 24%, and 16%, respectively. On the other hand, the content of random coils in vacuum, and in water with Ca^{2+} ions were 44.67%, and 68%, respectively. The stability of these protein structures is supported by additional information about the root-mean-square-deviation (RMSD) of protein structures, radius of gyration, and statistical hydrogen bond number (Figure S4 and Table S3). The simulation results on amorphous domain explain water and $CaCl_2$ introduce extensible structures in silk to improve stretchability. This is consistent with the Fourier-transformed infrared spectroscopy (FTIR) of plasticized silk films, which shows less β-sheets than pure silk films (Figure S5).

Based on the experimental and simulation results on the mechanical properties and underlying explanation inside silk protein, we have achieved the plasticization of original tough silk protein. This fulfils the materials requirement for the stretchable on-skin electronic devices. This work demonstrates that silk with $CaCl_2$ can possess skin-like mechanical

properties in ambient, although previous works demonstrate very soft silk gels incorporating much water and $CaCl_2$,[44] or stiff film by removing $CaCl_2$,[55] as summarized in Table S4. Furthermore, this work explains the plasticization mechanism by molecular dynamics simulation both in crystallite and amorphous domain, while previous simulation studies concentrate on how to increase the crystallite strength and there is few discussion on ions influence on silk protein from simulation.[46-49,51,52] Our study shows that water influences the crystallite strength, while ion does not. More importantly, the significant effect of ion together with water on amorphous domain was demonstrated, while further studies on ions interaction with chain can be explored.[56] Future development of more powerful simulation tools would bridge these correlation between microscale molecular dynamics simulation and macroscale experimental results. In addition, experimental studies have demonstrated the effect of plasticization can be observed by T_g shift after post-removal of $CaCl_2$.[57,58] These indicate $CaCl_2$ and water within silk would have significant influence on the mechanical properties.

The feasibility to integrate stretchable electronic devices on the plasticized silk was demonstrated by the simple vacuum deposition of metal films on plasticized silk. After the ambient hydration, the electrodes show a stretchability of >100% without affecting the original softness of plasticized silk (Figure S6). A 40 nm Au on stretchable silk showed a low initial sheet resistance of 7 Ohm/sq., and relative resistance change (R/R_0) of 2.45 at 40% strain, while control Au on polydimethylsilxane (PDMS) showed 20 Ohm/sq., and 31, respectively (**Figure 3**a). The lower initial sheet resistance is due to the uniform Au film formation on silk instead of microcracked Au on PDMS.[59,60] Furthermore, even if the Au thickness increased to 80 and 150 nm, the high stretchability of 100% was maintained and smaller sheet resistance was achieved (Figure 3a, and Figure S7). It is noteworthy that, in the microcracks based stretchable conductors such as Au on PDMS, increased Au thickness degrades the stretchability.[61] Furthermore, the high electrical performance was maintained

in the cyclic strains (100 cycles of 20% strain). The cycling durability was measured by laminating silk based electrodes on elastomer substrates in order to support the elastic recovery and mimic the situation in on-skin usage. During the cycles, the resistance varied from 10 Ω to 20 Ω, which is smaller than that of Au on PDMS (Figure 3b). In addition to Au, we also demonstrate other stable metals including Ag and Pt also become stretchable on our plasticized silk (Figure 3c). When Pt was sputtered on plasticized silk, and PDMS, stretchability of 60%, and 30% were obtained, respectively. Similarly, Ag on stretchable silk has achieved a high stretchability of 50%, while Ag on PDMS has achieved <10%. The hydrated phenomena can lead to metal oxidation so that only noble metals were adopted to form the conducting layers.

Optical microscope images of plasticized silk electrodes showed the stretchability originated from the wrinkles formation of metal films by the ambient hydration of stretchable silk substrates (Figure 3d-h). As-deposited electrodes showed a relatively flat surface (Figure 3d), yet, after the plasticization via ambient humidity, the electrodes formed wrinkled structures (Figure 3e). This hydration-induced wrinkles formation has been reported in different material systems,[62] but, to the best of our knowledge, this is the first report for realizing stretchable conductors by the substrate hydration. Until a strain of 40%, the wrinkles were extended, and microcracks started being formed (Figure 3f). This observation has a nice correlation with the small resistance change shown in Figure 3a. When the strain was 60%, no wrinkle was observed, and Au on silk started to form microcrack networks (Figure 3g). Further increase of strain increased the length and width of the cracks (Figure 3h), resulting in larger resistance change than wrinkles unfolding. It is noteworthy that the relationships between electrical performance and surface structures have a nice agreement with previous reports on wrinkles-based stretchable conductors.[63] They showed a stable electrical performance until wrinkles were unfolded and large resistance change when cracks were formed. This wrinkles-assisted stretchability was also confirmed in Ag and Pt on silk

substrates under ambient environment as shown in Figure S8. Utilizing the wrinkles formation, our stretchable silk realizes a simple fabrication of stretchable conductors with high conductivity and stretchability.

The softness and stretchability of our silk electrodes enabled highly skin-conformable electronics. **Figure 4**a shows that our electrodes were conformably laminated on skin while showing the high conductivity to operate a light emitting diode (LED) at a low voltage of 2.7 V. Further descriptions are available in experimental section and Figure S9. To improve the easiness to handle our soft silk electrodes while laminating on skin, devices were kept under relatively dry environment to make them rather stiff in advance. By moisturizing skin prior to the lamination, the electrodes can be immediately plasticized on skin, realizing conformal contacts to the skin. The high conformability was confirmed by cross-sectional scanning electron microscope (SEM) images of the silk electrodes laminated on skin replica (Figure 4b). No gap was observed between silk electrodes and skin microstructures. Furthermore, even with a smaller microstructured surface, our electrodes showed high conformability (Figure 4c). The adhesion strength with human skin was quantified by the 90° peeling tests, with experimental methods in supplementary information. The adhesion strength was as high as ~80 N/m, although that of commercial polyimide tape was ~50 N/m (Figure S10).

Finally, the advantage of our stretchable silk electrodes with biocompatibility and skin adhesiveness is demonstrated by the on-skin electrophysiological signals recording. Figure 4d shows the setup for skin interfacial impedance measurement and electromyography (EMG) recording by our plasticized silk electrodes on forearm skin. Our electrodes exhibited as low interfacial impedance with skin as commercial gel electrodes, which is crucial for the signal integrity in electrophysiological measurement (Figure 4e). The importance of conformal contact to skin was confirmed by attaching the Au side of silk electrodes to skin. The interfacial impedance increased in one order of magnitude. This result can be explained by the above-discussed high conformability to skins. In addition to the conformal contact, the

plasticized silk substrates contain water and Ca^{2+} ions which contribute to ionic conductivity between Au and skin. In this way, our plasticized silk serves the same function as the hydrogels in commercial EMG electrodes. Previous studies on long-term on-skin electrodes show higher interfacial impedance than commercial gel electrodes because they are normally dry.[15,20] Low impedance was achieved by the use of ionic liquid,[64] while our silk electrodes can provide low impedance by utilizing moisture in skin or ambient. The detected EMG signals achieved the amplitudes comparable to the signals collected by commercial gel electrodes (Figure 4f). The signal-to-noise ratios (SNR) obtained by silk electrodes, and commercial gel electrodes were 17.17 dB, and 17.95 dB, respectively. Furthermore, the accuracy of signals obtained by our silk electrodes was confirmed by amplitude-frequency spectrum, and energy spectrum analysis (Figure S11). In addition, the silk electrodes maintained the low interfacial impedance with skin even after 4 hours of wearing (Figure S12), and led to no remarkable skin irritation while commercial gel electrodes caused discomfort among 5 volunteers tested (Figure S13).

In conclusion, we have demonstrated the plasticization of silk protein for highly stretchable substrates in on-skin electronics. The plasticization of silk into skin-like softness was achieved by the addition of Ca^{2+} ions and the subsequent hydration via ambient humidity. The mechanisms of the plasticization were analyzed by molecular dynamics simulation, which are weakened strength of crystallite and more extensible secondary structures of amorphous domain. Furthermore, metal thin films on the silk form wrinkled structures during its plasticization by ambient humidity, resulting in highly conductive and stretchable electrodes. These features were fully utilized in on-skin electrophysiological electrodes. The softness of the silk substrates provides the conformal contact with skin, which enables low interfacial impedance with skin, and high-quality on-skin EMG signals recording. The plasticized silk will open up more progress in biomaterials-based wearable and implantable electronics with green features. For example, the silk electrodes will accelerate future

research on the integration of other active elements like sensors and transistors. We anticipate that the incorporation of biomaterials into wearable and implantable electronics will advance the harmonized integration between electronics and human.

Supporting Information
Supporting Information is available from the Wiley Online Library or from the author.

Acknowledgements
The authors thank the financial support from the National Research Foundation, Prime Minister's office, Singapore, under its NRF Investigatorship (NRF2016NRF-NRF1001-21), Singapore Ministry of Education (MOE2014-T2-2-140, MOE2015-T2-2-60), and K. C. Wong Education Foundation. YC and ZL are grateful for the supports from the Agency for Science, Technology and Research (A*STAR) and from A*STAR Computational Resource Centre, Singapore (ACRC).

Received: ((will be filled in by the editorial staff))
Revised: ((will be filled in by the editorial staff))
Published online: ((will be filled in by the editorial staff))

Reference

[1] D. H. Kim, J. A. Rogers, *Adv. Mater.* **2008**, *20*, 4887.

[2] J. A. Rogers, T. Someya, Y. Huang, *Science* **2010**, *327*, 1603.

[3] M. L. Hammock, A. Chortos, B. C. Tee, J. B. Tok, Z. Bao, *Adv. Mater.* **2013**, *25*, 5997.

[4] S. Choi, H. Lee, R. Ghaffari, T. Hyeon, D. H. Kim, *Adv. Mater.* **2016**, *28*, 4203.

[5] D. Qi, Z. Liu, W. R. Leow, X. Chen, *MRS Bull.* **2017**, *42*, 103.

[6] S. Wagner, S. Bauer, *MRS Bull.* **2012**, *37*, 207.

[7] D. H. Kim, J. Viventi, J. J. Amsden, J. Xiao, L. Vigeland, Y. S. Kim, J. A. Blanco, B. Panilaitis, E. S. Frechette, D. Contreras, D. L. Kaplan, F. G. Omenetto, Y. Huang, K. C. Hwang, M. R. Zakin, B. Litt, J. A. Rogers, *Nat. Mater.* **2010**, *9*, 511.

[8] P. Cai, W. R. Leow, X. Wang, Y. L. Wu, X. Chen, *Adv. Mater.* **2017**, *29*, 1605529.

[9] K. Ariga, J. Li, J. Fei, Q. Ji, J. P. Hill, *Adv. Mater.* **2016**, *28*, 1251.

[10] C. Sengottaiyan, R. Jayavel, P. Bairi, R. G. Shrestha, K. Ariga, L. K. Shrestha, *Bull. Chem. Soc. Jpn.* **2017**, *90*, 955.

[11] M. Kaltenbrunner, T. Sekitani, J. Reeder, T. Yokota, K. Kuribara, T. Tokuhara, M. Drack, R. Schwodiauer, I. Graz, S. Bauer-Gogonea, S. Bauer, T. Someya, *Nature* **2013**, *499*, 458.

[12] G. A. Holzapfel, *Mechanics of Biological Tissue*, Springer, Berlin, 2006.

[13] B. Zhu, H. Wang, Y. Liu, D. Qi, Z. Liu, H. Wang, J. Yu, M. Sherburne, Z. Wang, X. Chen, *Adv. Mater.* **2016**, *28*, 1559.

[14] R. C. Webb, A. P. Bonifas, A. Behnaz, Y. Zhang, K. J. Yu, H. Cheng, M. Shi, Z. Bian, Z. Liu, Y. S. Kim, W. H. Yeo, J. S. Park, J. Song, Y. Li, Y. Huang, A. M. Gorbach, J. A. Rogers, *Nat. Mater.* **2013**, *12*, 938.

[15] A. Miyamoto, S. Lee, N. F. Cooray, S. Lee, M. Mori, N. Matsuhisa, H. Jin, L. Yoda, T. Yokota, A. Itoh, M. Sekino, H. Kawasaki, T. Ebihara, M. Amagai, T. Someya, *Nat. Nanotech.* **2017**, *12*, 907.

[16] J. W. Jeong, W. H. Yeo, A. Akhtar, J. J. Norton, Y. J. Kwack, S. Li, S. Y. Jung, Y. Su, W. Lee, J. Xia, H. Cheng, Y. Huang, W. S. Choi, T. Bretl, J. A. Rogers, *Adv. Mater.* **2013**, *25*, 6839.

[17] Y. Liu, K. He, G. Chen, W. R. Leow, X. Chen, *Chem. Rev.* **2017**, *117*, 12893.

[18] T. Yamada, Y. Hayamizu, Y. Yamamoto, Y. Yomogida, A. Izadi-Najafabadi, D. N. Futaba, K. Hata, *Nat. Nanotech.* **2011**, *6*, 296.

[19] X. Wang, Y. Gu, Z. Xiong, Z. Cui, T. Zhang, *Adv. Mater.* **2014**, *26*, 1336.

[20] J. J. Norton, D. S. Lee, J. W. Lee, W. Lee, O. Kwon, P. Won, S. Y. Jung, H. Cheng, J. W. Jeong, A. Akce, S. Umunna, I. Na, Y. H. Kwon, X. Q. Wang, Z. Liu, U. Paik, Y. Huang, T. Bretl, W. H. Yeo, J. A. Rogers, *Proc. Natl. Acad. Sci. U. S. A.* **2015**, *112*, 3920.

[21] S.-W. Hwang, H. Tao, D.-H. Kim, H. Cheng, J.-K. Song, E. Rill, M. A. Brenckle, B. Panilaitis, S. M. Won, Y.-S. Kim, Y. M. Song, K. J. Yu, A. Ameen, R. Li, Y. Su, M. Yang, D. L. Kaplan, M. R. Zakin, M. J. Slepian, Y. Huang, F. G. Omenetto, J. A. Rogers, *Science* **2012**, *337*, 1640.

[22] M. Irimia-Vladu, E. D. Glowacki, G. Voss, S. Bauer, N. S. Sariciftci, *Mater. Today* **2012**, *15*, 340.

[23] J. Jin, D. Lee, H. G. Im, Y. C. Han, E. G. Jeong, M. Rolandi, K. C. Choi, B. S. Bae, *Adv. Mater.* **2016**, *28*, 5169.

[24] C. Vepari, D. L. Kaplan, *Prog. Polym. Sci.* **2007**, *32*, 991.

[25] Y. H. Jung, T. H. Chang, H. Zhang, C. Yao, Q. Zheng, V. W. Yang, H. Mi, M. Kim, S. J. Cho, D. W. Park, H. Jiang, J. Lee, Y. Qiu, W. Zhou, Z. Cai, S. Gong, Z. Ma, *Nat. Commun.* **2015**, *6*, 7170.

[26] E. Ruiz-Hitzky, M. Darder, P. Aranda, K. Ariga, *Adv. Mater.* **2010**, *22*, 323.

[27] F. G. Omenetto, D. L. Kaplan, *Science* **2010**, *329*, 528.

[28] D. N. Rockwood, R. C. Preda, T. Yucel, X. Wang, M. L. Lovett, D. L. Kaplan, *Nat. Protoc.* **2011**, *6*, 1612.

[29] J. Perez-Rigueiro, C. Viney, J. Llorca, M. Elices, *J. Appl. Polym. Sci.* **2000**, *75*, 1270.

[30] Z. Shao, F. Vollrath, *Nature* **2002**, *418*, 741.

[31] B. D. Lawrence, M. Cronin-Golomb, I. Georgakoudi, D. L. Kaplan, F. G. Omenetto, *Biomacromolecules* **2008**, *9*, 1214.

[32] S. T. Parker, P. Domachuk, J. Amsden, J. Bressner, J. A. Lewis, D. L. Kaplan, F. G. Omenetto, *Adv. Mater.* **2009**, *21*, 2411.

[33] B. Zhu, H. Wang, W. R. Leow, Y. Cai, X. J. Loh, M. Y. Han, X. Chen, *Adv. Mater.* **2016**, *28*, 4250.

[34] B. Kundu, R. Rajkhowa, S. C. Kundu, X. Wang, *Adv. Drug. Deliv. Rev.* **2013**, *65*, 457.

[35] H. Wang, B. Zhu, X. Ma, Y. Hao, X. Chen, *Small* **2016**, *12*, 2715.

[36] C. H. Wang, C. Y. Hsieh, J. C. Hwang, *Adv. Mater.* **2011**, *23*, 1630.

[37] H. Wang, F. Meng, B. Zhu, W. R. Leow, Y. Liu, X. Chen, *Adv. Mater.* **2015**, *27*, 7670.

[38] H. Wang, Y. Du, Y. Li, B. Zhu, W. R. Leow, Y. Li, J. Pan, T. Wu, X. Chen, *Adv. Funct. Mater.* **2015**, *25*, 3825.

[39] E. Steven, W. R. Saleh, V. Lebedev, S. F. Acquah, V. Laukhin, R. G. Alamo, J. S. Brooks, *Nat. Commun.* **2013**, *4*, 2435.

[40] B. P. Partlow, C. W. Hanna, J. Rnjak-Kovacina, J. E. Moreau, M. B. Applegate, K. A. Burke, B. Marelli, A. N. Mitropoulos, F. G. Omenetto, D. L. Kaplan, *Adv. Funct. Mater.* **2014**, *24*, 4615.

[41] M. Floren, C. Migliaresi, A. Motta, *J. Funct. Biomater.* **2016**, *7*, 26.

[42] H. Yuk, T. Zhang, G. A. Parada, X. Liu, X. Zhao, *Nat. Commun.* **2016**, *7*, 12028.

[43] X. Chen, *Small Methods* **2017**, *1*, 1600029.

[44] S. Ling, Q. Zhang, D. L. Kaplan, F. Omenetto, M. J. Buehler, Z. Qin, *Lab Chip* **2016**, *16*, 2459.

[45] S. Keten, Z. Xu, B. Ihle, M. J. Buehler, *Nat. Mater.* **2010**, *9*, 359.

[46] L. D. Koh, Y. Cheng, C. P. Teng, Y. W. Khin, X. J. Loh, S. Y. Tee, M. Low, E. Y. Ye, H. D. Yu, Y. W. Zhang, M. Y. Han, *Prog. Polym. Sci.* **2015**, *46*, 86.

[47] Y. Cheng, L. D. Koh, D. Li, B. Ji, M. Y. Han, Y. W. Zhang, *J. R. Soc. Interface* **2014**, *11*, 20140305.

[48] C. Xu, D. Li, Y. Cheng, M. Liu, Y. Zhang, B. Ji, *Acta. Mechanica. Sinica.* **2015**, *31*, 416.

[49] S. Xiao, W. Stacklies, M. Cetinkaya, B. Markert, F. Grater, *Biophys. J.* **2009**, *96*, 3997.

[50] D. Porter, F. Vollrath, Z. Shao, *Eur. Phys. J. E. Soft Matter.* **2005**, *16*, 199.

[51] S. Isabelle, M. J. Buehler, *Nanotechnology* **2016**, *27*, 302001.

[52] S. Y. Sheu, D. Y. Yang, H. L. Selzle, E. W. Schlag, *Proc. Natl. Acad. Sci. U. S. A.* **2003**, *100*, 12683.

[53] S. A. Fossey, G. Nemethy, K. D. Gibson, H. A. Scheraga, *Biopolymers* **1991**, *31*, 1529.

[54] C. Z. Zhou, F. Confalonieri, M. Jacquet, R. Perasso, Z. G. Li, J. Janin, *Proteins* **2001**, *44*, 119.

[55] F. Zhang, X. You, H. Dou, Z. Liu, B. Zuo, X. Zhang, *ACS Appl. Mater. Interfaces* **2015**, *7*, 3352.

[56] E. R. Morris, D. A. Rees, D. Thom, J. Boyd, *Carbohydr. Res.* **1978**, *66*, 145.

[57] F. Wang, H. Y. Yu, Z. G. Gu, L. Si, Q. C. Liu, X. Hu, *J. Therm. Anal. Calorim.* **2017**, *130*, 851.

[58] C. J. Fu, D. Porter, Z. Z. Shao, *Macromolecules* **2009**, *42*, 7877.

[59] M. Kyungtaek, U. Muhammad, R. Shinyoung, L. Soonil, K. Sunghwan, *Nanotechnology* **2017**, *28*, 115201.

[60] O. Graudejus, Z. Jia, T. Li, S. Wagner, *Scr. Mater.* **2012**, *66*, 919.

[61] T. Li, Z. Y. Huang, Z. Suo, S. P. Lacour, S. Wagner, *Appl. Phys. Lett.* **2004**, *85*, 3435.

[62] S. Zeng, R. Li, S. G. Freire, V. M. M. Garbellotto, E. Y. Huang, A. T. Smith, C. Hu, W. R. T. Tait, Z. Bian, G. Zheng, D. Zhang, L. Sun, *Adv. Mater.* **2017**, *29*, 1700828.

[63] S. P. Lacour, S. Wagner, Z. Y. Huang, Z. Suo, *Appl. Phys. Lett.* **2003**, *82*, 2404.

[64] P. Leleux, C. Johnson, X. Strakosas, J. Rivnay, T. Herve, R. M. Owens, G. G. Malliaras, *Adv. Healthc. Mater.* **2014**, *9*, 1377.

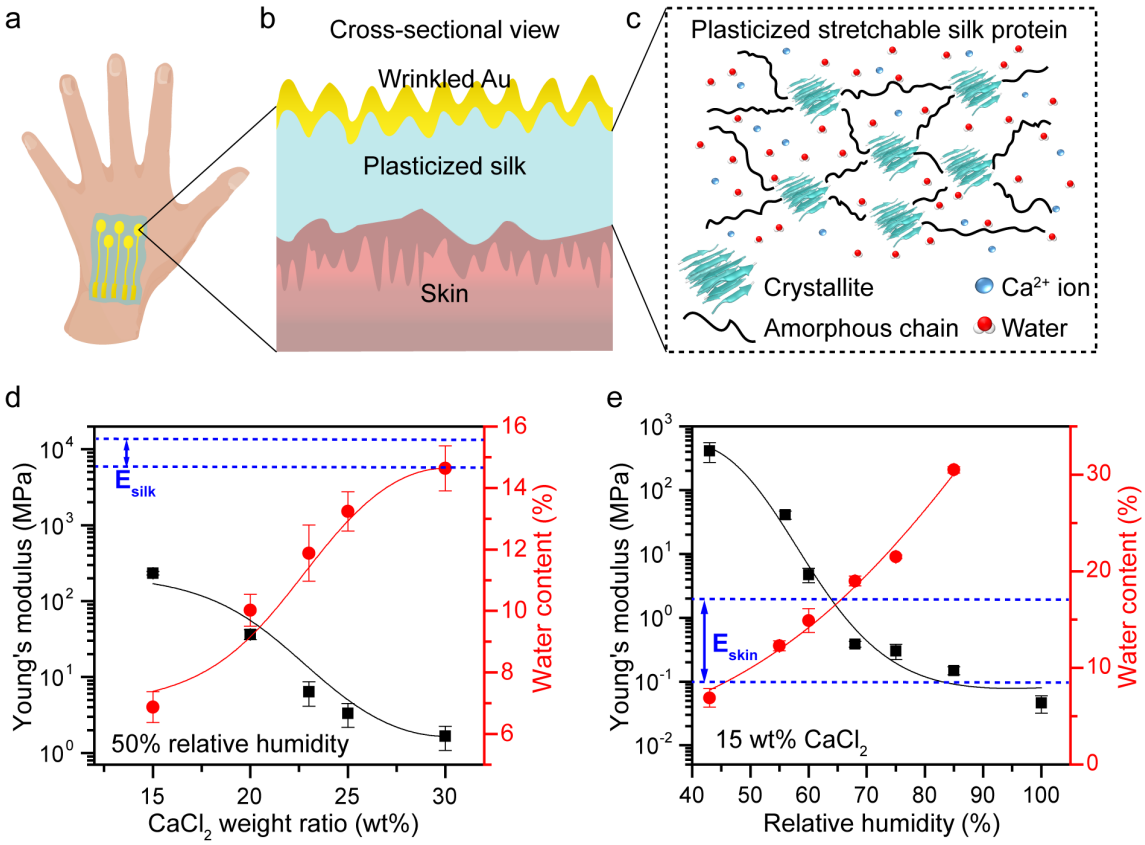

Figure 1. Plasticized silk proteins for on-skin electronics applications. a) A scheme of on-skin electrodes based on plasticized silk protein. b) A cross sectional scheme of the plasticized silk electrodes on skin, consisting of wrinkled Au and plasticized silk. c) A schematic of structural configuration inside the plasticized silk protein. d) The effect of $CaCl_2$ weight ratio in the Young's modulus (black) and the water content (red) under 50% relative humidity. e) The influence of relative humidity in the Young's modulus (black) and the water content (red). Plasticized silk film with 15 wt% $CaCl_2$ was used. Lines in d) and e) are eye guides.

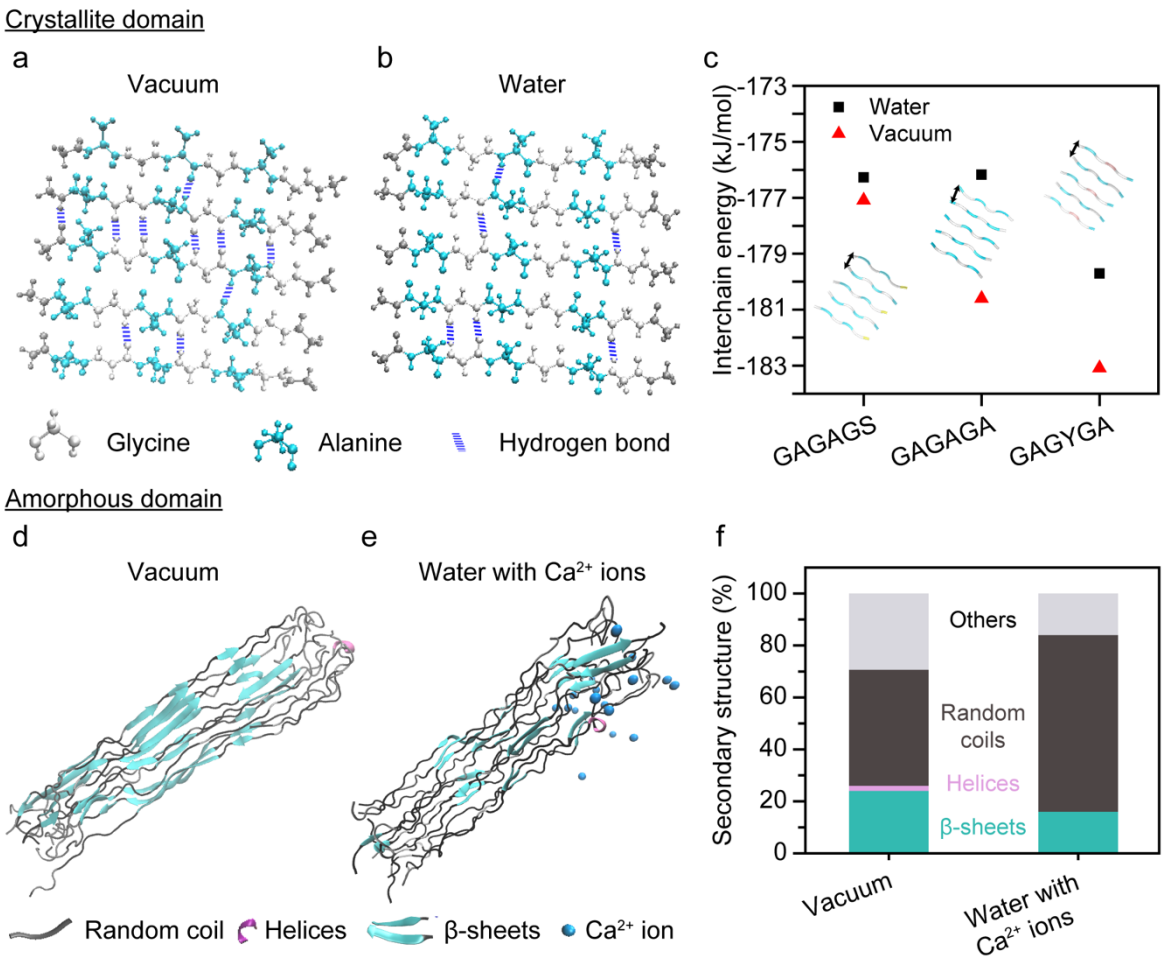

Figure 2. Molecular dynamics simulation to understand the plasticization mechanisms of silk protein. a,b) Representative snapshots of GAGAGA crystallites in vacuum, and water, respectively. c) The interchain energy of three typical crystallite structures (GAGAGS, GAGAGA, GAGYGA) in vacuum and water. d,e) Representative snapshots of amorphous domain in vacuum, and water with Ca^{2+} ions, respectively. In each of the environments, the silk forms different secondary structures (β-sheets, helices, random coils, and etc.), determining the extensibility of the molecules. f) Secondary structure ratio in the amorphous domain in vacuum and water with Ca^{2+} ions.

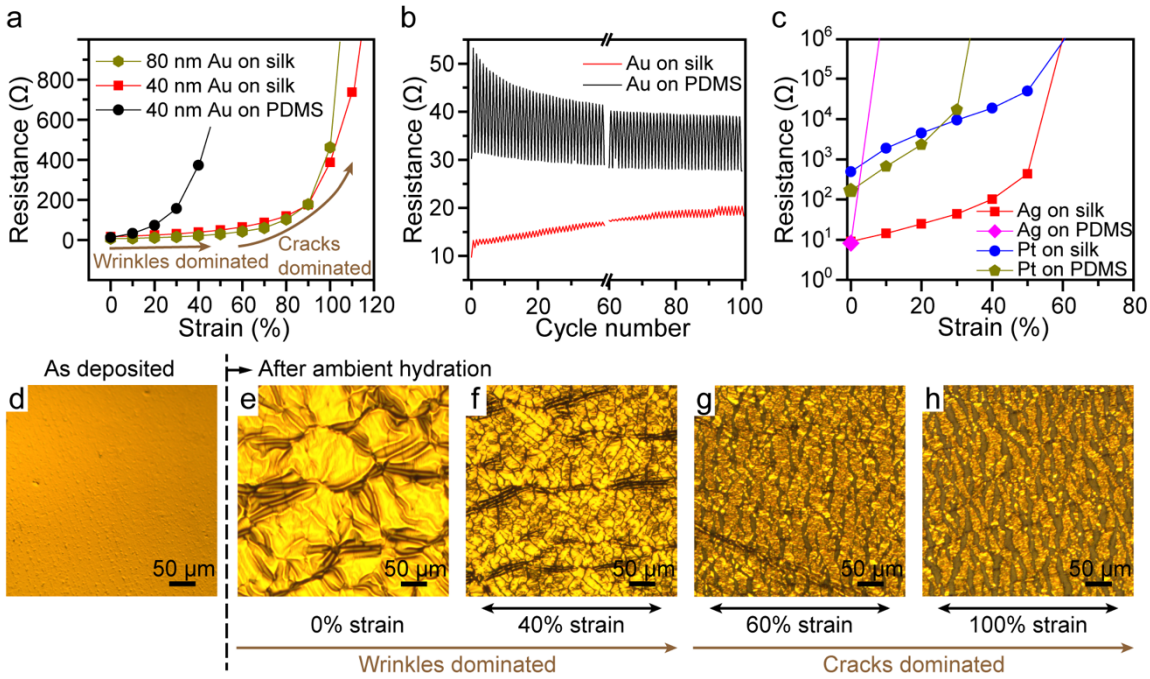

Figure 3. Electrical performance of the plasticized silk electrodes and the optical microscope images. a) Resistance-strain characteristics of Au (40 and 80 nm) on plasticized silk, and Au (40 nm) on PDMS. b) Resistance change of silk electrodes and PDMS electrodes under cyclic 20% strain. c) Resistance-strain characteristics of Pt and Ag on plasticized silk and PDMS. d-h) Optical microscope images of Au on plasticized silk under different situations: right after the Au deposition (d); after ambient hydration (e); and under strains of 40% (f); 60% (g); 100% (h). The thickness of Au is 80 nm and the relative humidity is 60%.

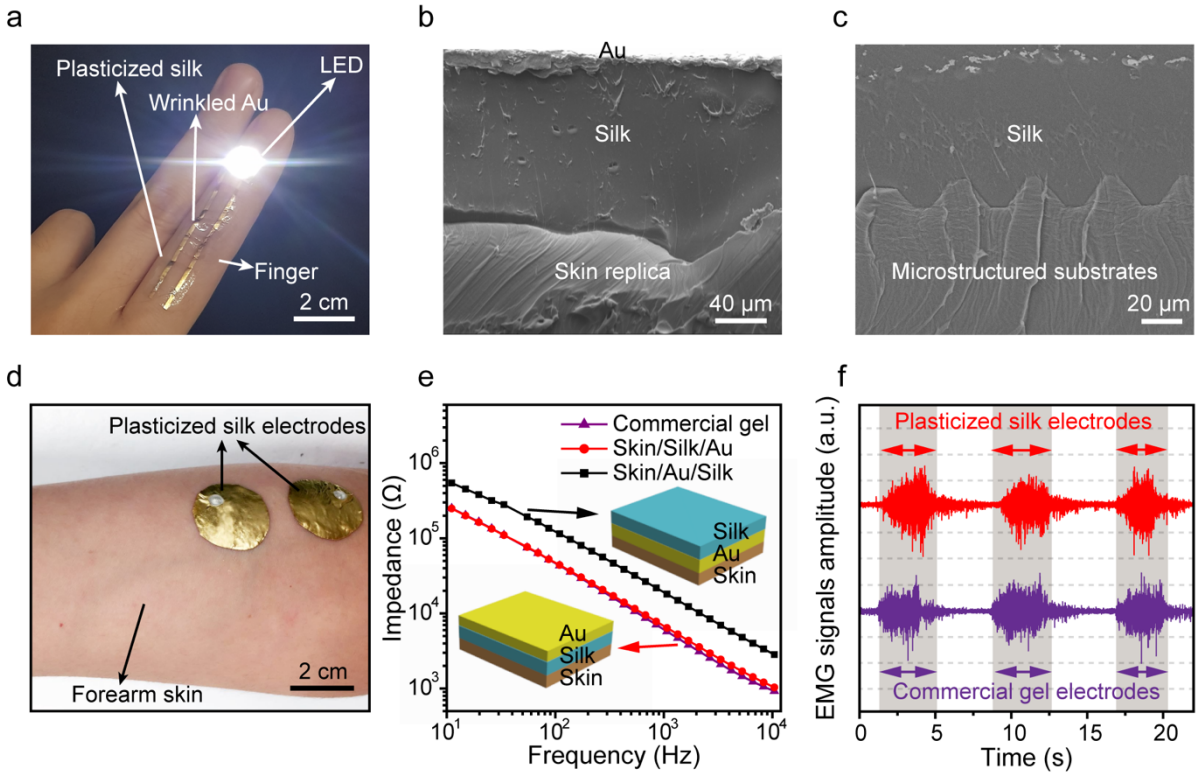

Figure 4. High conformability of plasticized silk electrodes to skin structures and the on-skin electronics application. a) Photographic image of plasticized silk electrodes conformably attached on a finger skin. The conductance of the electrodes is as high as an LED can be operated in 2.7 V. b,c) Cross-sectional SEM image of the plasticized silk electrodes attached on skin replica, and microstructured substrates, respectively. d) A photographic image of an EMG measurement setup using plasticized silk electrodes laminated on a human forearm. e) On-skin interfacial impedance of the plasticized silk electrodes in comparison with commercial gel electrodes. The results were obtained when the silk sides were laminated (Skin/Silk/Au) and Au side were laminated (Skin/Au/Silk). f) EMG signals obtained by the plasticized silk electrodes and commercial gel electrodes. Two-direction arrows describe when motions happened.

Silk protein is plasticized, and demonstrated as soft and stretchable substrates for the skin-conformable stretchable electronics. The plasticization is enabled by the addition of $CaCl_2$ and ambient hydration, whose mechanism is investigated by molecular dynamics simulation. Moreover, highly stretchable (>100%) silk electrodes are fabricated for on-skin electrophysiological measurement. This progress opens up more biomaterials based wearable electronics.

Biomaterials, Silk protein, Molecular dynamics simulation, On-skin electronics, Stretchable electronics

G. Chen, N. Matsuhisa, Z. Liu, D. Qi, P. Cai, Y. Jiang, C. Wan, Y. Cui, W. R. Leow, Z. Liu, S. Gong, K. Q. Zhang, Y. Cheng*, X. Chen*

Plasticizing Silk Protein for On-skin Stretchable Electrodes

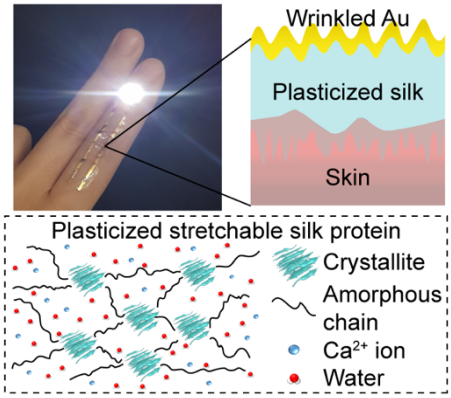

Supporting Information

Plasticizing Silk Protein for On-skin Stretchable Electrodes

Geng Chen, Naoji Matsuhisa, Zhiyuan Liu, Dianpeng Qi, Pingqiang Cai, Ying Jiang, Changjin Wan, Yajing Cui, Wan Ru Leow, Zhuangjian Liu, Suxuan Gong, Ke-Qin Zhang, Yuan Cheng, Xiaodong Chen**

Experimental Section

Plasticization of silk protein: 10 g *Bombyx mori* silk fibers were boiled in 0.02 M Na_2CO_3 distilled water solution for 1 hour, and rinsed thoroughly with distilled water in order to remove the sericin.[S1] The degummed silk fibers were dried in oven for 2 days under 60°C. The dried fibers were then dissolved in formic acid with $CaCl_2$,[S2] followed by ultrasonication to totally dissolve the fibroin fibers and remove bubbles. The weight ratio of $CaCl_2$ to silk was changed from 15% to 30%. Finally, the solution were poured to petri dishes and dried in fume hoods for overnight evaporation of formic acid.

Measurement of Young's Modulus and stretchability of plasticized silk: Stress-strain curves were obtained by a mechanical tester (C42, MTS Systems Corporation) with environmental chamber (Bionix Environbath, MTS Systems Corporation) to control the relative humidity. The relative humidity was tuned by placing saturated salt solution (KCl, NaCl, KI, NaBr, K_2CO_3) in the chamber overnight, and the relative humidity values were estimated according to the partial pressure of saturated salt solutions. The humidity of ambient environment was measured by commercial humidity meter HI 9565 (HANNA Instruments). Tensile tests were conducted for more than three samples for each of the conditions at a speed of 2 mm/min. The Young's modulus was calculated using the first 0.5% strain region.

Molecular dynamics simulations of crystallites domain:All the simulations for crystallites and amorphous domain were conducted by the software package GROMACS 4.5.5.[S3] using the force field set of Amber 03.[S4] First, the models for crystallite domain were built, which are three anti-parallel β-sheet crystallite units (GAGAGA, GAGYGA, and GAGAGS) representing the crystal domains of *Bombyx mori* silk.[S5] They contain repeating 3 layers and 5 chains as a typical crystallite. The initial structure of GAGAGA crystallite was obtained from Protein Data Bank Entry (2slk),[S6] and the initial structures of GAGYGA and GAGAGS were mutated through Chimera[S7] by replacing the A to S or Y on the first layer. For the simulation of the crystallite units in water, the systems were solvated in a water box with a dimension of 3.6 × 3.6 × 2.8 nm^3. A model of transferable intermolecular potential with 3 points (TIP3P) was adopted for the water.[S8] In addition, energy minimization was carried out to obtain the equilibrium status both in vacuum and in water. Finally, molecular dynamics simulation were performed to the pre-equilibrated systems under 100 ns of Canonical ensemble (NVT) at a temperature at 300 K and 100 ns of Isothermal-isobaric (NPT) ensemble[S9] at a temperature of 300 K and pressure of 1 bar both in vacuum and water. The boundary condition was set to periodic. The time step to collect data was 0.002 ps. The long-range electrostatic interactions were calculated by particle mesh Ewald (PME) method.[S10] The criteria for judging whether there is a hydrogen bond between a hydrogen atom and a hydrogen bond acceptor was set to that the distance is within 0.35 nm and the bonding angle is less than 30°. The interchain energies were calculated from two chains in the edge of the outmost layer of crystallites as the representative pair (described by two-direction arrows in Figure 2c). Representative snapshots for protein configuration were produced using software visualized molecular dynamics (VMD) Molecular Graphics Viewer.[S11]

Molecular dynamics simulations of amorphous domain: The initial structures for amorphous domain were built based on the silk fibroin sequence according to the Linker 6 as published

by Zhou et al: (GAGAGAGAGAGTGSSGFGPYVANGGYSGYEYAWSSESDFGTGS).[S12] The initial structure of the amorphous domain consisted of 12 fully-extended amorphous chain. These amorphous chains were arranged in an antiparallel manner with an initial distance of 5 Å between adjacent chains, followed by energy minimization to the initial structure. After that, 500 ns of stochastic dynamics simulation in implicit solvent was carried out on the structure to obtain the pre-equilibrated amorphous domain. The following molecular dynamics simulation was carried out based on this pre-equilibrated amorphous domain in vacuum and in water with Ca^{2+} ions, respectively. For the simulation of the amorphous domain in water with Ca^{2+} ions, the systems were first solvated in explicit water box with a dimension of $4 \times 4 \times 11.2$ nm^3. A model of transferable intermolecular potential with 3 points (TIP3P) was adopted for the water.[S8] Then, 18 Ca^{2+} ions were added to replace some of the water molecules to neutralize the system. In addition, another energy minimization was carried out to obtain the equilibrium status both in vacuum and in water with Ca^{2+} ions. Finally, molecular dynamics simulation was performed to the pre-equilibrated systems under 100 ns of Canonical ensemble (NVT) at a temperature of 300 K and 100 ns Isothermal-isobaric (NPT) ensemble at a temperature of 300 K and pressure of 1 bar both in vacuum and water with Ca^{2+} ions.[S9] Secondary structures of protein were analyzed using the STRIDE algorithm,[S13] which is a built-in module in the VMD Molecular Graphics Viewer. All the representative snapshots for protein configuration were produced using VMD Molecular Graphics Viewer.[S11]

Infrared Spectroscopy (FTIR) measurements: All the FTIR spectra were obtained using the FTIR spectrometer (The PerkinElmer Frontier™ IR) with Attenuated Total Reflectance (ATR) accessories from the wavenumber of 4000 cm^{-1} to 1000 cm^{-1}. The silk films with different $CaCl_2$ weight ratios were cut into 1 cm^2 to be tested. The absorption intensities were

normalized according to the peak of random coils at 1646 cm^{-1}. And the peak of β-sheets was analyzed at 1625 cm^{-1}. [S14]

Fabrication of stretchable electrodes on plasticized silk protein: Prior to the metal depositions, silk films with $CaCl_2$ were dried in the oven at 60°C for 1 h to remove the water. Au and Ag thin films were formed by a vacuum thermal evaporator (Nano 36, Kurt J. Lesker) under $2x10^{-6}$ Torr at a deposition rate of 0.3 Å/s. The Au and Ag sources were purchased from Kurt J. Lesker and the purity was 99.99%. Pt was sputtered by JFC-1600 auto fine coater for 240 s at 40 mA. After the depositions, samples were hydrated under 60% relative humidity for overnight. As a control, PDMS films were prepared by mixing the precursor and cross linker at 10: 1 ratio, spin coating on top of fluorinated silicon wafer at 1000 rpm, and curing under 60°C for 4 h. All the metal films were deposited simultaneously on both silk films and PDMS films.

Measurements of resistance change under strain: All the tests were performed under 60% relative humidity, and the sample sizes were united to 2 cm (length) × 1 cm (width). The resistance was measured by a semiconductor parameter analyzer (Keithley 4200-SCS, Tektronix) while strains were applied by a manual tensile stage. For the measurement of resistance under cyclic strains, 20% strain was applied using a mechanical tester at a speed of 2 mm/min while the resistance was recorded by a semiconductor parameter analyzer (Keithley 4200-SCS, Tektronix).

LED integration with plasticized silk electrodes: A plasticized silk electrode and chip LED (5050, 3M™) were attached on a finger. A double-side tape was used to fix the LED. The plasticized silk electrode was connected with the LED and power generator (SPS-3610, GW Instek) using copper wires and Ga-In eutectic (Sigma-Aldrich). In order to light up the LED,

a voltage of 2.7 V was applied from the power generator. The wiring setup is shown in Figure S9.

90° peeling tests of the adhesion strength between our plasticized electrodes and skin: The methods followed and modified the previously reported procedure.[S15] The Au side of our plasticized electrodes were glued with a polyimide sheet (RS Components, Singapore) by using super glue in order to eliminate the effect of substrate deformation. The widths were 1 cm. Water mists were then applied to our forearm skin, and the electrodes with polyimide sheets were attached to skin with one end released. The released end was gripped to a mechanical tester (C42, MTS Systems Corporation) to detect the peeling force at a speed of 6 mm/min. The adhesion strength was calculated dividing the force by the width of the electrodes.

Cross sectional SEM observation: The skin replica was fabricated by casting PDMS onto the forearm texture mold (P&G Singapore LTD.). Microstructured surface was prepared by casting PDMS onto the Si pyramidal mold which was fabricated by reported anisotropic etching process on silicon wafer.[S16] These surfaces were treated with short O_2 plasma to improve the hydrophilicity, and were sprayed with water mist before laminating silk electrodes. Then, the cross section was obtained by cutting whole the layers using sharp razor blades. SEM images were obtained through Zeiss Supra 55 SEM at an acceleration voltage of 10 kV under secondary electron image (SEI) mode.

Skin interfacial impedance measurement and EMG signals recording: The interfacial impedance was measured by laminating pairs of electrodes with a circle shape (diameter: 2 cm), and a center-to-center distance of 5 cm on forearm skin. As the electrodes, plasticized silk electrodes and commercial gel electrodes (Large muscle electrodes, Backyard Brains)

were used. The interfacial impedance measurements were conducted using electrochemical workstation (ZAHNER ZENNIUM) from 1 Hz to 1 MHz with a voltage of 100 mV. EMG signals were obtained while bending the wrist towards the body at 90° for 3 s and the signals were recorded by a toolkit for EMG recording (Muscle Spikerbox, Backyard Brain). The test was approved by Institute of Review Board, Nanyang Technological University (approval number: IRB-2017-08-035). The toolkit includes amplifier and 50/60 Hz filter. SNR were obtained through the equation (1): [S17]

$$SNR = 10 * \log 10(P_{signal} - P_{noise})/P_{noise}) \quad (1)$$

P_{signal}, and P_{noise} denote the signal intensity, and background noise level, respectively. They were calculated from the obtained signals by the previously reported algorithm.[S16]

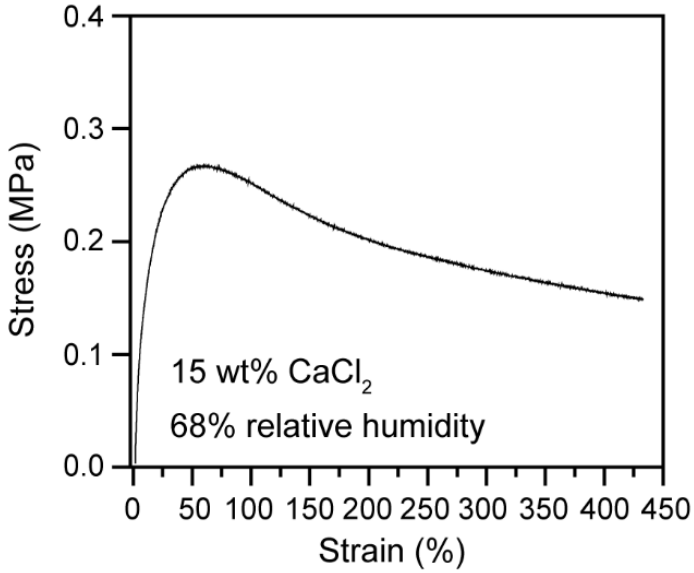

Figure S1. The tensile stress-strain curve of plasticized silk protein showing more than 400% stretchability. 15 wt% $CaCl_2$ and relative humidity of 68% were adopted here.

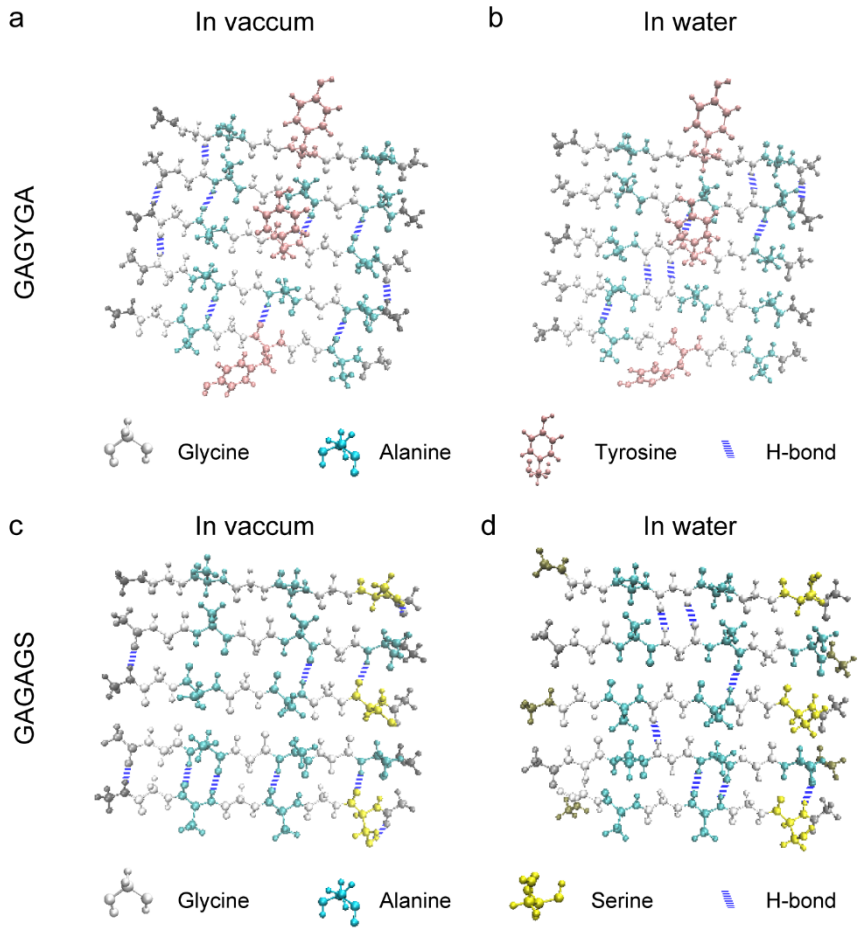

Figure S2. Representative snapshots of crystallites in vacuum and in water. a, b) Typical snapshots of crystallites of GAGYGA in vacuum (a), and in water (b). c,d) Typical snapshots of crystallites of GAGAGS in vacuum (c), and in water (d).

Table S1. Statistical hydrogen bond number of whole crystallites. (The data were collected during the last 50 ns after equilibrium)

Crystallite	In vacuum	In water
GAGAGA	83.5 ± 1.4	73.9 ± 2.7
GAGYGA	83.6 ± 1.4	78.1 ± 3.0
GAGAGS	86.3 ± 1.4	71.9 ± 2.7

Table S2. Statistical hydrogen bond number between the two chains on the outmost layer of each crystallites in water with and without Ca^{2+} ions. (The data were collected during the last 50 ns after equilibrium)

Crystallite	In water without Ca^{2+} ions	In water with Ca^{2+} ions
GAGAGA	6.1 ± 0.9	6.2 ± 0.8
GAGYGA	6.2 ± 0.8	6.2 ± 0.8
GAGAGS	6.2 ± 0.8	6.2 ± 0.8

Table S3. Statistical hydrogen bond number of amorphous domain in vacuum and in water with Ca^{2+} ions at equilibrium. (The data were collected during the last 50 ns after equilibrium)

	In vacuum	In water with Ca^{2+} ions
Hydrogen bond number	452.5 ± 9.1	251.9 ± 10.4

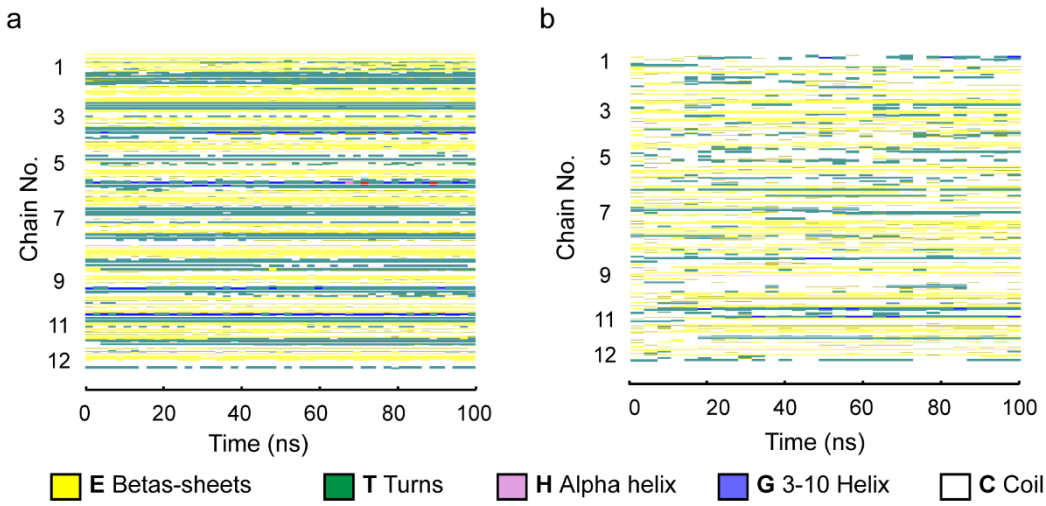

Figure S3. Time evolution of secondary structures (Timeline analysis) of 12 peptide chains in amorphous domain in vacuum (a), and in water with Ca^{2+} ions (b). Each of the chains contains 43 residues.

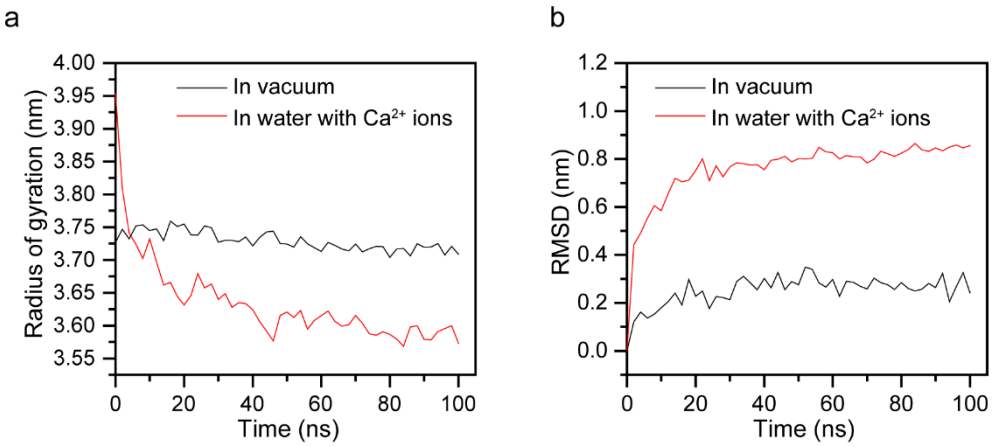

Figure S4. Structural stability of the amorphous domain. a) Radius of gyration of amorphous domain in vacuum and in water with Ca^{2+} ions. The stable values after 50 ns showed the structural equilibration. b) Root-mean-square-deviation (RMSD) of amorphous domain of silk protein in vacuum and in water with Ca^{2+} ions. The plateaus of RMSD which were less than 1 nm showed the protein structures were at equilibrium.

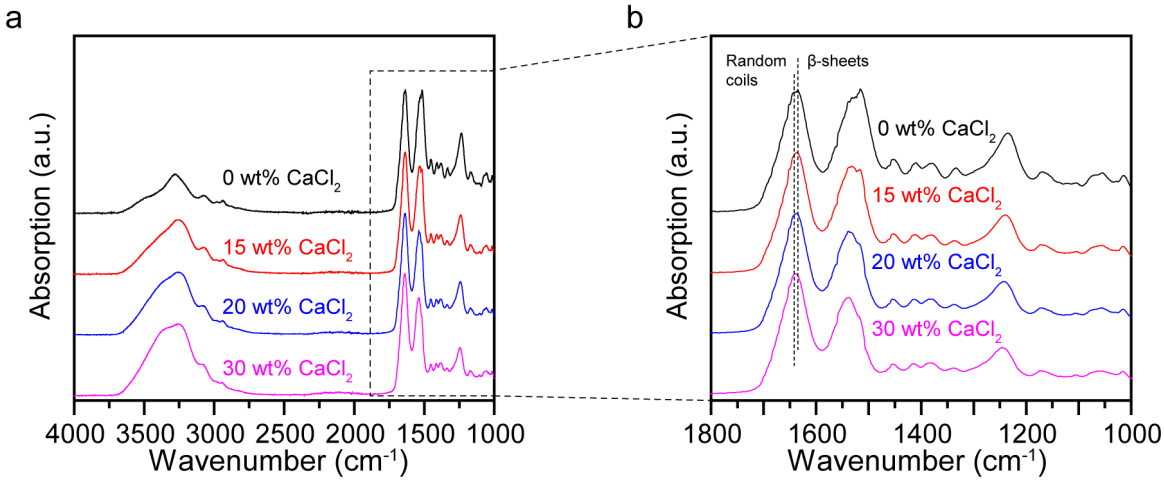

Figure S5. FTIR absorbance spectra of pure silk film, silk film with 15 wt% $CaCl_2$, 20% $CaCl_2$ and 30% $CaCl_2$ at the range from 4000 cm^{-1} to 1000 cm^{-1} (a), and 1800 cm^{-1} to 1000 cm^{-1} (b). Relative humidity was set to 50%. With the addition of $CaCl_2$, data in a shows the increased water peak intensity (4000 ~3000 cm^{-1}), and data in b shows a peak shift from 1625 cm^{-1} to 1646 cm^{-1}.

Table S4. Comparison of Young's modulus of silk film from various methods.

Methods	Young's modulus	Ref
Raw silk fibers	5~12 GPa	S18
Ultrathin film	6~8 GPa	S19
As cast silk fibroin film	3.9 GPa	S20
$CaCl_2$-FA dissolved silk, $CaCl_2$ removed (Wet)	206 MPa	S21
Water annealing film	22.0 MPa	S22
Methanol-treated	18.7 MPa	S22
$CaCl_2$-FA dissolved silk, with $CaCl_2$	0.102 MPa (together with pig skin)	S2
$CaCl_2$-FA dissolved silk, with $CaCl_2$ (Under ambient)	0.149 ~ 412.67 MPa	This work

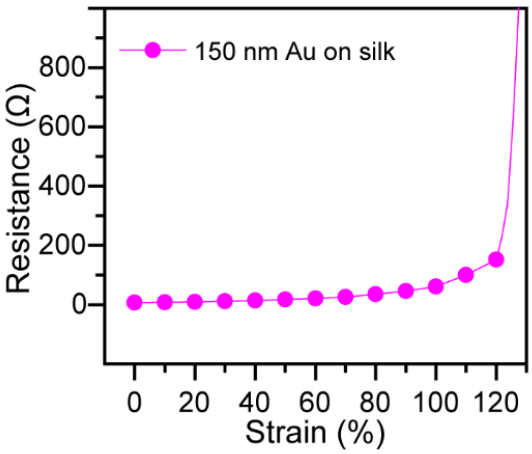

Figure S6. Resistance-strain characteristics of 150 nm Au on plasticized silk protein.

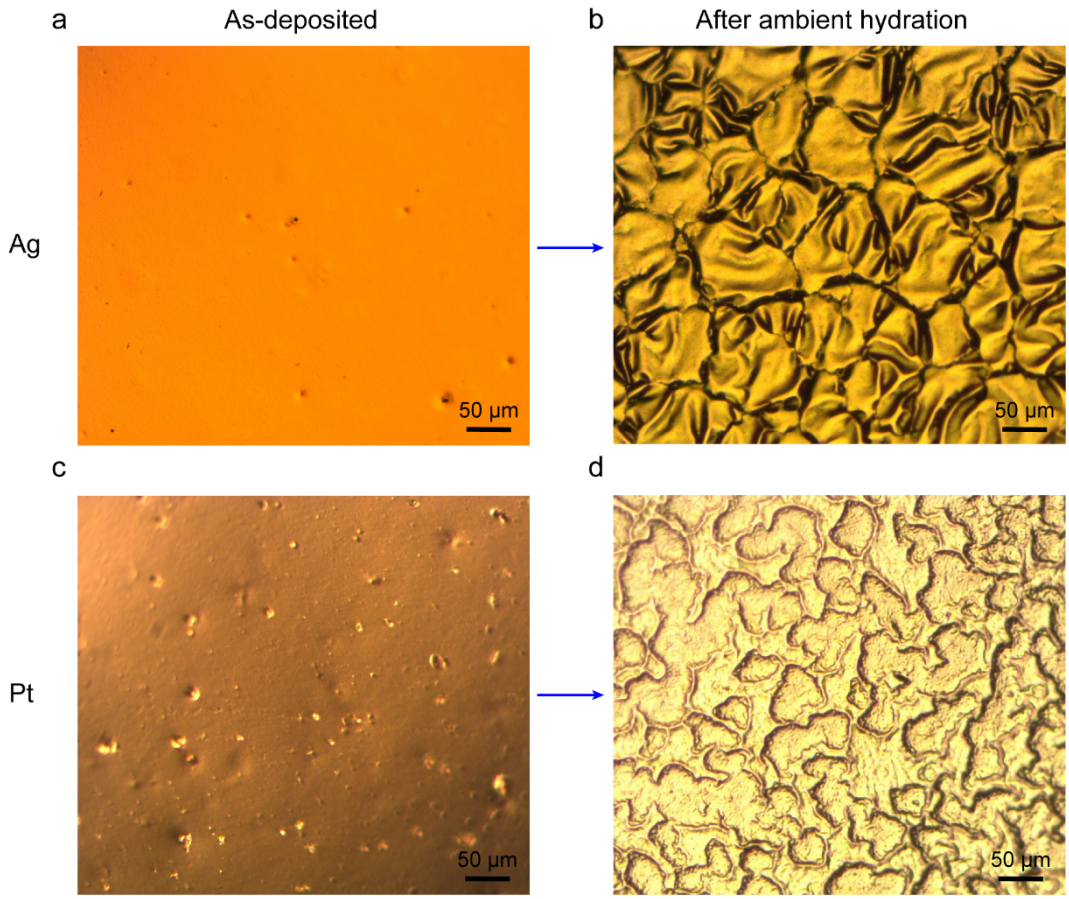

Figure S7. Optical microscopic of various metal films on our plasticized silk film under different situations: As deposited Ag (a) and Pt (c) on plasticized silk; Ag (b), and Pt (d) on plasticized silk after ambient hydration.

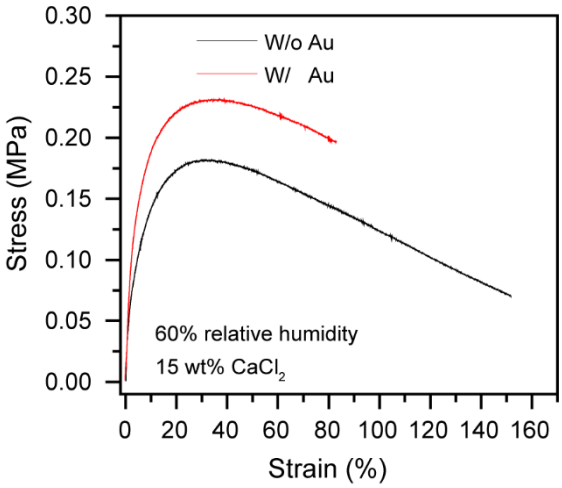

Figure S8. Mechanical tensile curve of pure plasticized silk protein (w/o Au) and silk electrodes (w/ 80 nm Au) under relative humidity of 60%, showing the comparable softness.

a

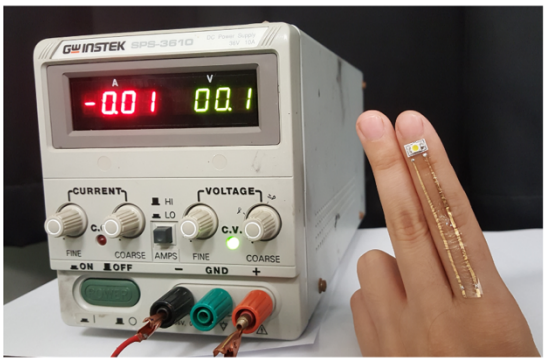

Without applying voltage

b

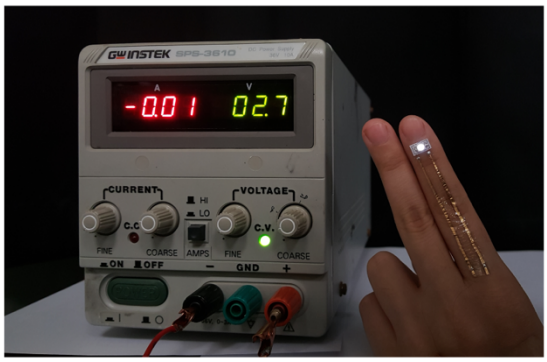

Applying voltage of 2.7 V

Figure S9. a) The photograph of LED connected with power source without applying voltage by our on-skin silk electrodes. b) The photograph of LED connected with power source applying 2.7 V voltage by our on-skin silk electrodes.

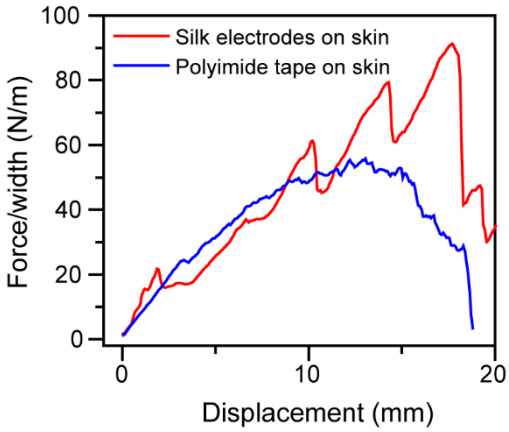

Figure S10. 90° peeling test of a plasticized silk electrode and polyimide tape from skin, showing their adhesion strength with skin.

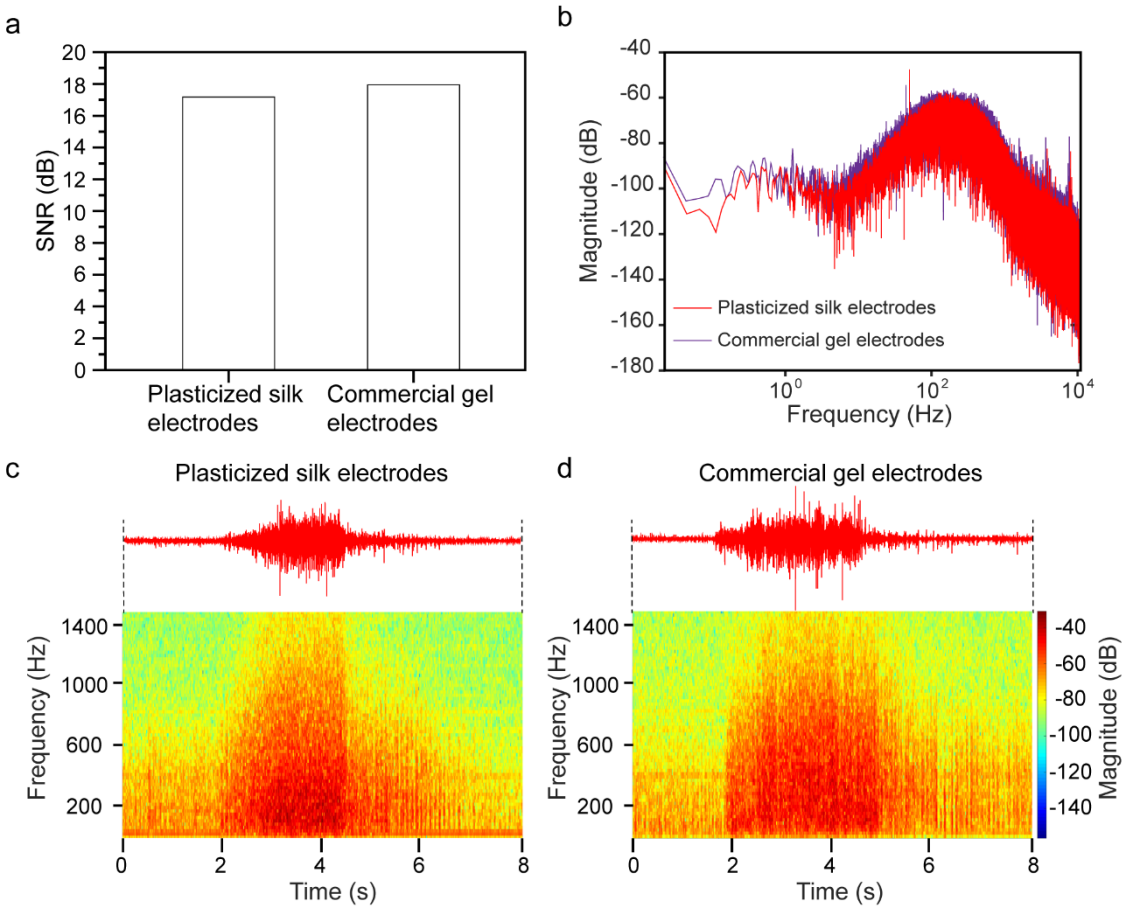

Figure S11. Comparison between the EMG signals from our plasticized silk electrodes and commercial gel electrodes. a) Signal-to-noise ratio (SNR) of the EMG signal detected by plasticized silk electrodes and commercial gel electrodes. b) Amplitude spectrum of the EMG signals recorded by plasticized silk electrodes and commercial gel electrodes. c,d) Energy spectrum analysis of the EMG signals recorded by plasticized silk electrodes (c), and commercial gel electrodes (d).

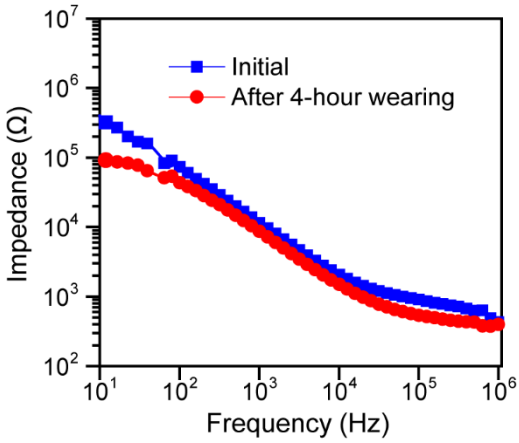

Figure S12. On-skin interfacial impedance of plasticized silk electrodes after 4-hour wearing in comparison with initial interfacial impedance.

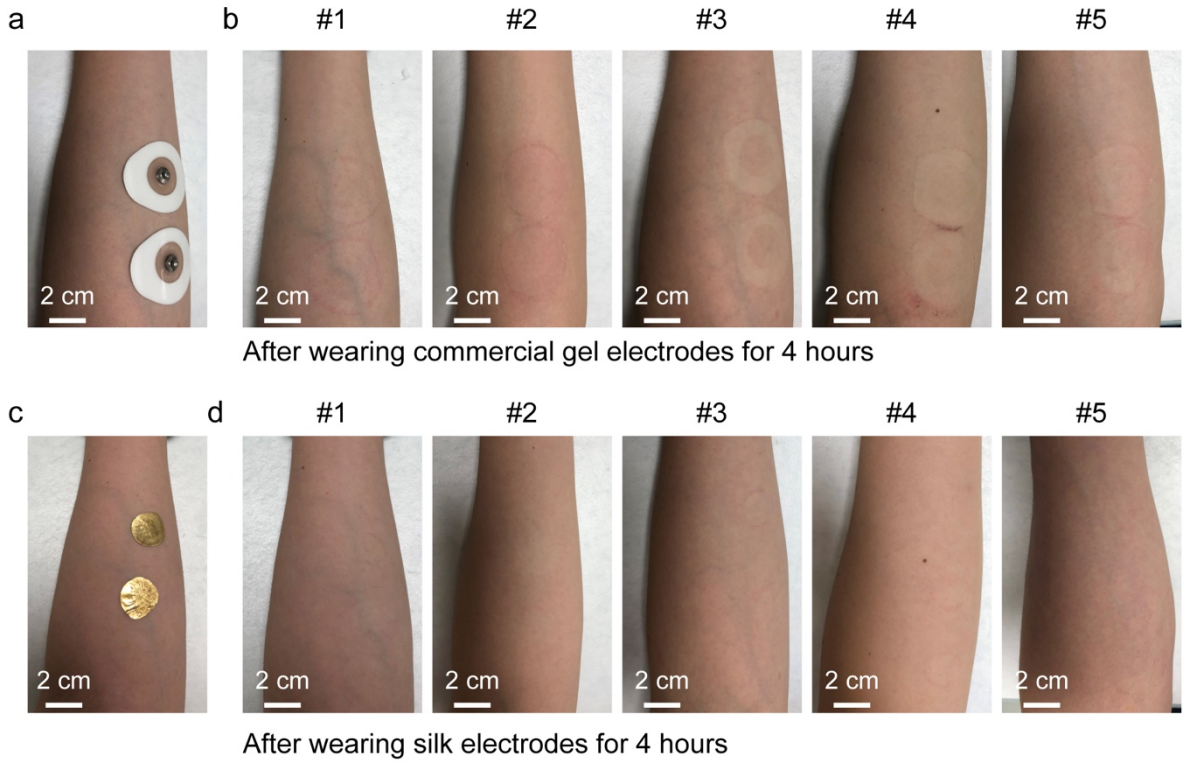

Figure S13. a) Skin inflammation was observed after wearing commercial gel electrodes for 4 hours. b) No skin inflammation was observed after wearing our plasticized silk electrodes for 4 hours.

Reference

[S1] D. N. Rockwood, R. C. Preda, T. Yucel, X. Wang, M. L. Lovett, D. L. Kaplan, *Nat. Protoc.* **2011**, *6*, 1612.

[S2] S. Ling, Q. Zhang, D. L. Kaplan, F. Omenetto, M. J. Buehler, Z. Qin, *Lab Chip* **2016**, *16*, 2459.

[S3] D. Van Der Spoel, E. Lindahl, B. Hess, G. Groenhof, A. E. Mark, H. J. Berendsen, *J. Comput. Chem.* **2005**, *26*, 1701.

[S4] Y. Duan, C. Wu, S. Chowdhury, M. C. Lee, G. Xiong, W. Zhang, R. Yang, P. Cieplak, R. Luo, T. Lee, J. Caldwell, J. Wang, P. Kollman, *J. Comput. Chem.* **2003**, *24*, 1999.

[S5] L. D. Koh, Y. Cheng, C. P. Teng, Y. W. Khin, X. J. Loh, S. Y. Tee, M. Low, E. Y. Ye, H. D. Yu, Y. W. Zhang, M. Y. Han, *Prog. Polym. Sci.* **2015**, *46*, 86.

[S6] S. A. Fossey, G. Nemethy, K. D. Gibson, H. A. Scheraga, *Biopolymers* **1991**, *31*, 1529.

[S7] E. F. Pettersen, T. D. Goddard, C. C. Huang, G. S. Couch, D. M. Greenblatt, E. C. Meng, T. E. Ferrin, *J. Comput. Chem.* **2004**, *25*, 1605.

[S8] W. L. Jorgensen, J. Chandrasekhar, J. D. Madura, R. W. Impey, M. L. Klein, *J. Chem. Phys.* **1983**, *79*, 926.

[S9] H. J. C. Berendsen, J. P. M. Postma, W. F. Vangunsteren, A. Dinola, J. R. Haak, *J. Chem. Phys.* **1984**, *81*, 3684.

[S10] T. Darden, D. York, L. Pedersen, *J. Chem. Phys.* **1993**, *98*, 10089.

[S11] W. Humphrey, A. Dalke, K. Schulten, *J. Mol. Graph.* **1996**, *14*, 33.

[S12] C. Z. Zhou, F. Confalonieri, M. Jacquet, R. Perasso, Z. G. Li, J. Janin, *Proteins* **2001**, *44*, 119.

[S13] M. Heinig, D. Frishman, *Nucleic Acids Res.* **2004**, *32*, W500.

[S14] X. Chen, Z. Shao, N. S. Marinkovic, L. M. Miller, P. Zhou, M. R. Chance, *Biophys. Chem.* **2001**, *89*, 25.

[S15] H. Yuk, T. Zhang, G. A. Parada, X. Liu, X. Zhao, *Nat. Commun.* **2016**, *7*, 12028.

[S16] B. Zhu, Z. Niu, H. Wang, W. R. Leow, H. Wang, Y. Li, L. Zheng, J. Wei, F. Huo, X. Chen, *Small* **2014**, *10*, 3625.

[S17] V. Agostini, M. Knaflitz, *IEEE Trans. Biomed. Eng.* **2012**, *59*, 219.

[S18] C. Vepari, D. L. Kaplan, *Prog. Polym. Sci.* **2007**, *32*, 991.

[S19] C. Y. Jiang, X. Y. Wang, R. Gunawidjaja, Y. H. Lin, M. K. Gupta, D. L. Kaplan, R. R. Naik, V. V. Tsukruk, *Adv. Funct. Mater.* **2007**, *17*, 2229.

[S20] H. J. Jin, J. Park, V. Karageorgiou, U. J. Kim, R. Valluzzi, D. L. Kaplan, *Adv. Funct. Mater.* **2005**, *15*, 1241.

[S21] F. Zhang, X. You, H. Dou, Z. Liu, B. Zuo, X. Zhang, *ACS Appl. Mater. Interfaces* **2015**, *7*, 3352.

[S22] B. D. Lawrence, S. Wharram, J. A. Kluge, G. G. Leisk, F. G. Omenetto, M. I. Rosenblatt, D. L. Kaplan, *Macromol. Biosci.* **2010**, *10*, 393.